01 Mar 2022

Transition Metal-Catalyzed and MAO-Assisted Olefin Polymerization. Cyclic Isomers of Sinn's Dimer Are Excellent Ligands in Iron Complexes and Great Methylating Reagents

Kaidi Yang

Rainer Glaser
Missouri University of Science and Technology, glaserr@mst.edu

Recommended Citation

K. Yang and R. Glaser, "Transition Metal-Catalyzed and MAO-Assisted Olefin Polymerization. Cyclic Isomers of Sinn's Dimer Are Excellent Ligands in Iron Complexes and Great Methylating Reagents," *Catalysts*, vol. 12, no. 3, article no. 312, MDPI, Mar 2022.
The definitive version is available at https://doi.org/10.3390/catal12030312

catalysts

MDPI

Article

Transition Metal-Catalyzed and MAO-Assisted Olefin Polymerization; Cyclic Isomers of Sinn's Dimer Are Excellent Ligands in Iron Complexes and Great Methylating Reagents

Kaidi Yang [1] and Rainer Glaser [1,2,*]

[1] Department of Chemistry, University of Missouri, Columbia, MO 65211, USA; kyn69@umsystem.edu
[2] Department of Chemistry, Missouri University of Science & Technology, Rolla, MO 65409, USA
* Correspondence: glaserr@umsystem.edu

Abstract: Methylaluminoxane (MAO) is the most commonly used co-catalyst for transition metal-catalyzed olefin polymerization, but the structures of MAO species and their catalytic functions remain topics of intensive study. We are interested in MAO-assisted polymerization with catalysts $L(R_2)FeCl_2$ (L = tridentate pyridine-2,6-diyldimethanimine; imine-R = Me, Ph). It is our hypothesis that the MAO species is not merely enabling Fe–Me bond formation but functions as an integral part of the active catalyst, a MAO adduct of the Fe-precatalyst $[L(R_2)FeCl]^+$. In this paper, we explored the possible structures of acyclic and cyclic MAO species and their complexation with pre-catalysts $[L(R_2)FeCl]^+$ using quantum chemical approaches (MP2 and DFT). We report absolute and relative oxophilicities associated with the Fe ← O(MAO) adduct formation and provide compelling evidence that oxygen of an acyclic MAO species (i.e., $O(AlMe_2)_2$, **4**) cannot compete with the O-donor in cyclic MAO species (i.e., $(MeAlO)_2$, **7**; $MeAl(OAlMe_2)_2$, cyclic **5**). Significantly, our work demonstrates that intramolecular O → Al dative bonding results in cyclic isomers of MAO species (i.e., cyclic **5**) with high oxophilicities. The stabilities of the $[L(R_2)FeCl_{ax}(MAO)_{eq}]^+$ species demonstrate that **5** provides for the ligating benefits of the cyclic MAO species **4** without the thermodynamically costly elimination of TMA. Mechanistic implications are discussed for the involvement of such Fe–O–Al bridged catalyst in olefin polymerization.

Keywords: methylaluminoxane (MAO); oxophilicity; iron pre-catalyst; olefin polymerization; molecular modeling; pre-catalyst MAO adduct

Citation: Yang, K.; Glaser, R. Transition Metal-Catalyzed and MAO-Assisted Olefin Polymerization: Cyclic Isomers of Sinn's Dimer Are Excellent Ligands in Iron Complexes and Great Methylating Reagents. *Catalysts* **2022**, *12*, 312. https://doi.org/10.3390/catal12030312

Academic Editors: Carl Redshaw and Gregory A. Solan

Received: 11 February 2022
Accepted: 6 March 2022
Published: 9 March 2022

1. Introduction

Ziegler-Natta polymerization [1,2] is the dominant method for the production of polyolefin [3,4]. Ziegler-Natta catalysts usually contain transition metal complexes (i.e., $TiCl_4$) and partially hydrolyzed aluminum alkyls as co-catalyst, among which methylaluminoxane [5–7] (MAO) is most commonly used today [8–10]. It was a major advance in the field when Brookhart discovered that Fe(II) complexes with di-nitrogen or tri-nitrogen ligands can serve as pre-catalyst with satisfying catalytic activity [11–13]. More recently, Sun and co-workers explored structurally similar bidentate bis(imino)pyridyl Fe(II) complexes [14], and tridentate 2,8-bis(imino)quinoline Fe(II) complexes [15], and related systems with nickel [16–18], cobalt [19,20], and titanium [21,22] also have been studied. However, these kinds of pre-catalysts require the presence of a very large excess of MAO as co-catalyst (>2000:1) and the structure and the function of MAO have not been clarified at all [23]. The experimental studies of aluminoxanes by Barron [24,25], Pasynkiewicz [26], and Sinn [27] suggested a plethora of chain, ladder, and cage structures. Theoretical studies by Ziegler et al. [28], by Hall and co-workers [29], and by Linnolahti et al. [30,31] explored possible species with ladder and cage structures derived from dimethylaluminum hydroxide (DMAH).

Most of the MAO studies have described very large MAO structures and it was believed that these very large MAO structures also are the active co-catalysts [32,33]. We hold a different view and hypothesize that initially formed MAO species of moderate size are the active co-catalysts and that the large excess required merely reflects the fact that small MAO species tend to aggregate into larger and catalytically less or non-active species. We have published a theoretical study [34] of the formation of varies MAO species (Scheme 1) by partial hydrolysis of trimethylaluminum (TMA) **1**. Here we are exploring the possible function of small MAO species as co-catalysts.

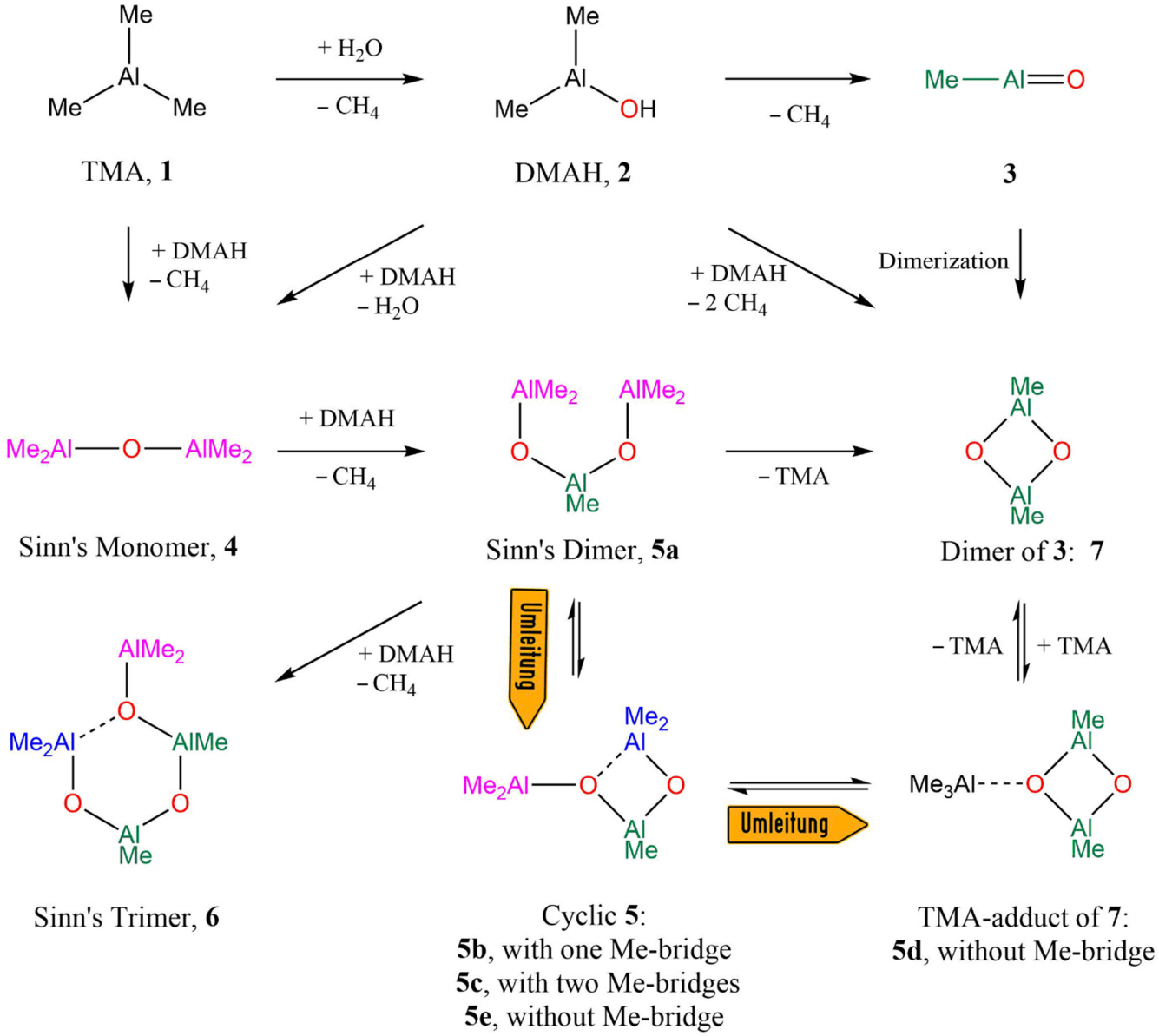

Scheme 1. Possible Products Formed by Partial Hydrolysis of Trimethylaluminum **1**. Methyl-Transfer Isomerization of **5a** Provides a Path to Cyclic **5** and the TMA Adduct of **7** without Going Through **3**.

In Scheme 2, three mechanisms of catalysis are outlined for a generic $LFeCl_2$ pre-catalyst, where L signifies a tri-nitrogen ligand. All of them share the feature that at least one chloride is abstracted to generate an overall positively charged Fe(II) complex. The abstracted "first" chloride might aggregate with a MAO species and form a large "A^-" anion which associated with the iron complex, and this scenario is shown in the top row. In this commonly considered mechanism [35], the next step consists in the replacement of

the second chloride by a methyl anion (from MAO) forming an Fe–Me bond. After this alkylation step and on entry of an alkene into the vacant coordination site, a nucleophilic addition of the methyl anion to the coordinated alkene results in the replacement of the methyl anion ligand by a propyl anion ligand, and so on. Alternatively, one may consider mechanisms in which the MAO species *does not alkylate* the transition metal and instead *coordinates to* the transition metal (Scheme 2, center and bottom) and create a Fe–O–Al bridged catalyst. After their coordination to the transition metal, the MAO species would transfer a methyl group directly from Al to the olefin.

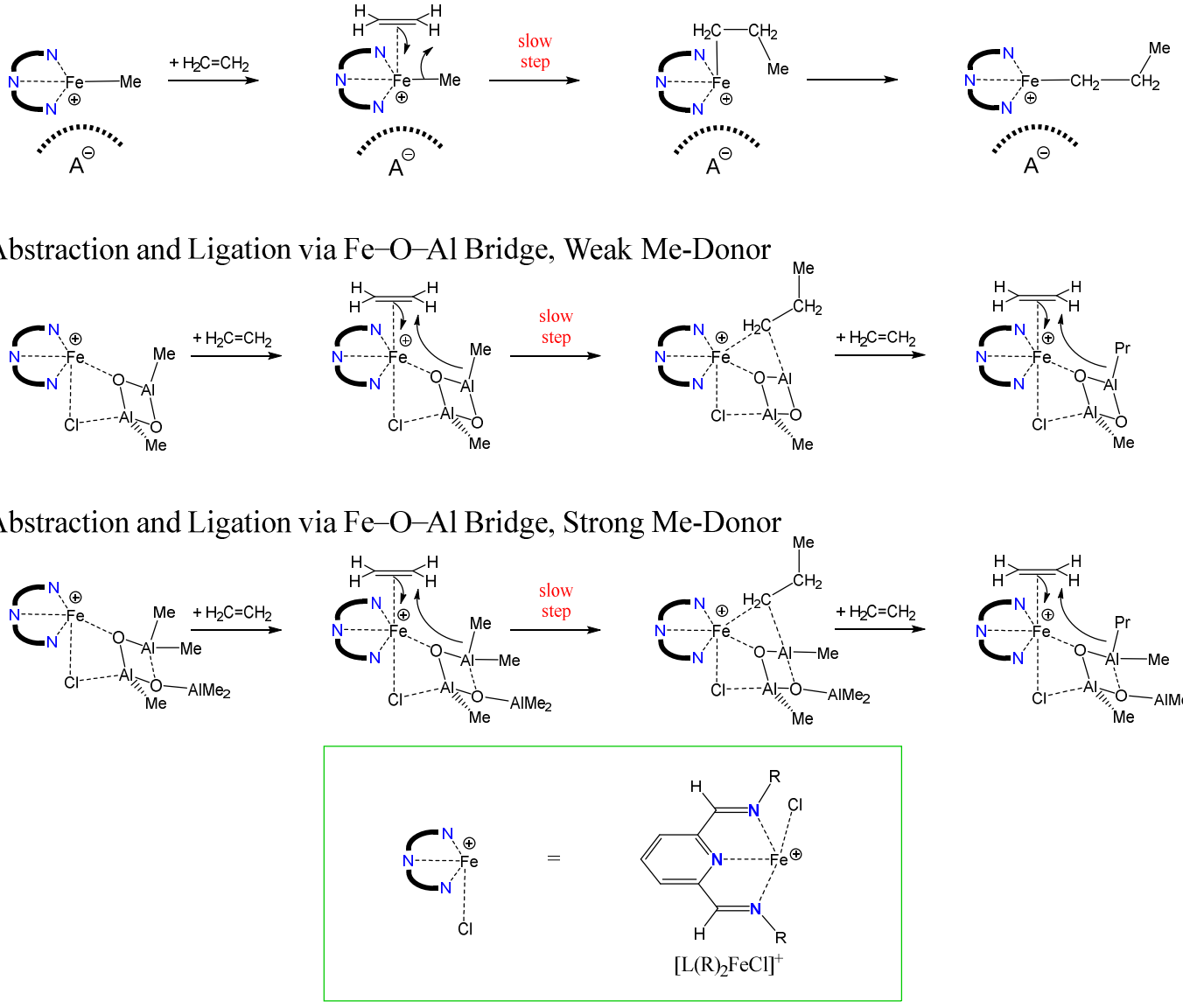

Scheme 2. Mechanisms of Different MAO Co-Catalysts Catalyzing Olefin Polymerization.

An Al-based alkylation mechanism with Fe–O(MAO) bonding should discriminate strongly between acyclic and cyclic aluminoxanes (Scheme 3). The bridging oxygen in an acyclic aluminoxane may engage both of its p-lone pairs to engage in O → Al dative bonding. This is illustrated by resonance forms **4-IIa**, **4-IIb**, and **4-III** in Scheme 3 for $Me_2Al–O–AlMe_2$ (R = Me). The strength of this O → Al dative bonding may be reduced by coordination of other donors to Al, but it will not be eliminated. Therefore, any O → Fe dative bonding in a complex of an acyclic species will always have to compete with two options for O → Al dative bonding. Cyclodialuminoxane **7** exemplifying cyclic MAO species in Scheme 2. Each oxygen in a cyclic aluminoxane can only engage its out-of-plane

p-lone pair p_{oop} for O → Al dative bonding and, thus, the one in-plane σ-lone pair σ_{ip} will be available for O → Fe dative bonding. We will substantiate this argument below and it is for that reason that the mechanisms shown in Scheme 1 involve cyclic MAO species. The consideration of cyclodialuminoxane as the active co-catalyst warrants the study of two possible issues. First, the formation of cyclodialuminoxane **7** from the Sinn dimer **5a** by TMA elimination might not be able to compete with oligomerization of the Sinn dimer **5a** to the Sinn trimer **6**. Second, the Fe-coordinated cyclodialuminoxane **7** is only a weak methyl donor.

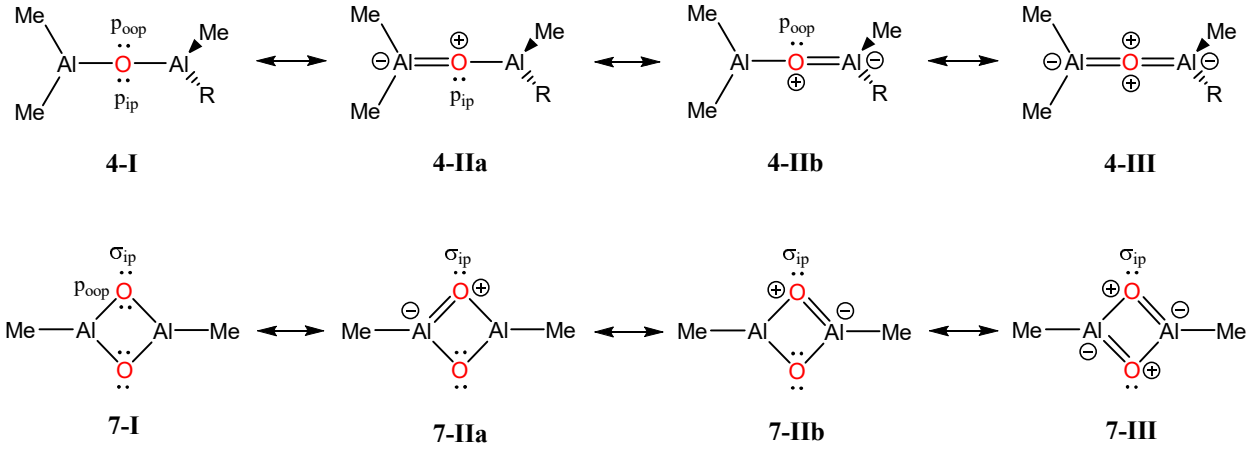

Scheme 3. Differences in Intramolecular O → Al σ-Dative Bonding in Acyclic and Cyclic Aluminoxanes Affect Their Capacity to Serve as Lewis Acceptors and Lewis Donors in Intermolecular Interactions.

Here we report on the thermochemistry of the formation of the Sinn dimer **5** from the Sinn monomer **4**. Detailed exploration of the potential energy surface of **5** reveals that the acyclic Sinn dimer structure **5a** can rearrange easily into cyclic isomers **5b** and **5c**, which effectively are TMA-complexed cyclodialuminoxane, **7**•TMA. We then discuss the ligand binding capacities of acyclic **4**, cyclic **7**, and cyclic **5** with Fe^{2+} complexes of type $[L(R_2)FeCl]^+$. The organic ligand L is the tridentate pyridine-2,6-diyldimethanimine and we studied the *N*,*N*-diphenyl ligand $L(Ph)_2$ and the *N*,*N*-dimethyl ligand $L(Me)_2$. The structures of the $[L(R_2)FeCl(MAO)]^+$ species show that the **5** is a much better Me-donor than **4**, and $[L(R_2)FeCl(\mathbf{5})]^+$ illustrates well the mechanism shown in the bottom row of Scheme 2. The stabilities of the $[L(R_2)FeCl(MAO)]^+$ species demonstrate that **5** provides for the ligating benefits of the cyclic MAO species **4** without the thermodynamically costly elimination of TMA.

2. Results and Discussion

Isomer preference energies, activation, and reaction energies are discussed, and we report relative energies ΔE, enthalpies, $\Delta H_0 = \Delta(E + \text{VZPE})$ and $\Delta H_{298} = \Delta(E + \text{TE})$, and free enthalpies $\Delta G_{298} = \Delta(E + \text{TE} - 298.153 \cdot \text{S})$. Results for the MAO species are collected in Table 1 and all relevant energy of complexation chemistry are collected in Table 2. Computated energies of MAO species and the iron pre-catalyst are shown in Tables S1 and S2. Structures of optimized MAO species are shown in Figures S1–S3. Cartesian coordinates of all the stationary structures are shown in the supporting information.

Table 1. Computed Relative and Reaction Energies of Formation of Permethyltrialuminoxane **5** and Isomerization of **5** (kcal/mol).

Reaction/Process	E	ΔH_0	ΔH_{298}	ΔG_{298}
5a → **5b** (Cyclization)	−9.86	−8.73	−10.25	−0.64
5b → **5c**	−0.95	−0.67	−1.04	0.78
5a → **5c** (Cyclization)	−10.82	−9.40	−11.29	0.14
E_{act}, TSRF(**5a**,**5b**) vs. **5a**	1.57	1.67	0.80	5.63
E_{act}, TSMT(**5b**,**5c**) vs. **5b**	0.12	0.06	−0.56	1.57
E_{act}, ATS(*5c*) vs. **5c**	21.58	20.39	20.93	16.74
DMAH (**2**) + TMA (**1**) → **4** + CH_4	−49.14	−48.20	−47.63	−46.16
4 + **2** → **5a** + CH_4	−48.05	−47.26	−46.64	−45.38
4 + **2** → **5c** + CH_4	−58.87	−56.66	−57.93	−45.24
4 + MeAlO (**3**) → **5c**	−98.87	−96.27	−97.03	−79.69
4 + 0.5 $(MeAlO)_2$ (**7**) → **5c**	−32.22	−30.78	−31.58	−18.71

Table 2. Computed Relative and Reaction Energies (kcal/mol, B3LYP/6-31G *).

Rxn.	Reaction/Process	ΔE	ΔH_0	ΔH_{298}	ΔG_{298}
	N-phenyl ligands $L(Ph)_2$				
1	$L(Ph)_2FeCl_2$, $C_2 \rightarrow C_s$	0.02	0.03	0.03	−0.18
2	$[L(Ph)_2FeCl]^+$, I → II	3.58	0.43	0.47	0.62
3	$[L(Ph)_2FeCl]^+$, I → III	0.59	0.43	0.47	0.62
4	$[L(Ph)_2FeCl_{ax}(\mathbf{4})_{eq}]^+ \rightarrow [L(Ph)_2FeCl_{eq}(\mathbf{4})_{ax}]^+$	4.15	4.06	4.14	3.84
5	$[L(Ph)_2FeCl_{ax}(\mathbf{7})_{eq}]^+ \rightarrow [L(Ph)_2FeCl_{eq}(\mathbf{7})_{ax}]^+$	3.83	3.65	3.82	2.82
6	$[L(Ph)_2FeCl_{ax}(\mathbf{5})_{eq}]^+ \rightarrow [L(Ph)_2FeCl_{eq}(\mathbf{5})_{ax}]^+$	−4.66	−4.72	−4.74	−4.57
7	$[L(Ph)_2FeCl]^+$ + **4** → $[L(Ph)_2FeCl_{eq}(\mathbf{4})_{ax}]^+$	−34.60	−33.00	−32.68	−14.96
8	$[L(Ph)_2FeCl]^+$ + **4** → $[L(Ph)_2FeCl_{ax}(\mathbf{4})_{eq}]^+$	−38.75	−37.06	−36.82	−18.80
9	$[L(Ph)_2FeCl]^+$ + **7** → $[L(Ph)_2FeCl_{eq}(\mathbf{7})_{ax}]^+$	−50.29	−49.02	−48.49	−32.56
10	$[L(Ph)_2FeCl]^+$ + **7** → $[L(Ph)_2FeCl_{ax}(\mathbf{7})_{eq}]^+$	−54.12	−52.67	−52.31	−35.38
11	$[L(Ph)_2FeCl]^+$ + **5** → $[L(Ph)_2FeCl_{eq}(\mathbf{5})_{ax}]^+$	−54.22	−53.40	−52.29	−39.55
12	$[L(Ph)_2FeCl]^+$ + **5** → $[L(Ph)_2FeCl_{ax}(\mathbf{5})_{eq}]^+$	−49.56	−48.69	−47.55	−34.97
	N-methyl ligands $L(Me)_2$				
13	$[L(Me)_2FeCl_{ax}(\mathbf{4})_{eq}]^+ \rightarrow [L(Me)_2FeCl_{eq}(\mathbf{4})_{ax}]^+$	5.06	4.62	4.90	4.62
14	$[L(Me)_2FeCl_{ax}(\mathbf{7})_{eq}]^+ \rightarrow [L(Me)_2FeCl_{eq}(\mathbf{7})_{ax}]^+$	−0.33	−0.62	−0.43	−1.73
15	$[L(Me)_2FeCl_{ax}(\mathbf{5})_{eq}]^+ \rightarrow [L(Me)_2FeCl_{eq}(\mathbf{5})_{ax}]^+$	−3.10	−3.39	−3.29	−3.41
16	$[L(Me)_2FeCl]^+$ + **4** → $[L(Me)_2FeCl_{eq}(\mathbf{4})_{ax}]^+$	−40.51	−38.87	−38.57	−21.44
17	$[L(Me)_2FeCl]^+$ + **4** → $[L(Me)_2FeCl_{ax}(\mathbf{4})_{eq}]^+$	−45.57	−43.49	−43.47	−26.06
18	$[L(Me)_2FeCl]^+$ + **7** → $[L(Me)_2FeCl_{eq}(\mathbf{7})_{ax}]^+$	−54.33	−53.17	−52.53	−38.27
19	$[L(Me)_2FeCl]^+$ + **7** → $[L(Me)_2FeCl_{ax}(\mathbf{7})_{eq}]^+$	−53.99	−52.54	−52.09	−36.53
20	$[L(Me)_2FeCl]^+$ + **5** → $[L(Me)_2FeCl_{eq}(\mathbf{5})_{ax}]^+$	−58.65	−57.83	−56.69	−44.70
21	$[L(Me)_2FeCl]^+$ + **5** → $[L(Me)_2FeCl_{ax}(\mathbf{5})_{eq}]^+$	−55.55	−54.44	−53.41	−41.28

2.1. Formation of Sinn Dimer **5** *and Its Structural Isomerization*

The most likely path for the formation of trialuminoxane **5** is outlined in Scheme 1, stationary structures of **5** are shown in Figure 1, and relevant energies are collected in Table 1. Acyclic trialuminoxane **5a** can be formed from **4** by adding DMAH and losing methane. The reaction energy ΔG_{298} = −45.4 kcal/mol for this intermolecular CH_4 elimination between DMAH and **4** to form **5a** is very similar to the respective value of ΔG_{298} = −41.2 kcal/mol for the reaction of DMAH and TMA.

The acyclic structure **5a** features two near-linear Al–O–Al moieties indicative of a strong O → Al π-dative bonding. Structure **5a** can stabilize itself by intramolecular O → Al σ-dative bond formation and resulting in minimum **5b** (Figure 1). The cyclization energy of **5** is just about compensated by the loss in cyclization entropy, and **5b** is only 0.6 kcal/mol more stable than **5a**. The additional O–Al contact (1.91 Å) is only slightly longer than a normal O–Al bond (1.8 Å) and the exocyclic $AlMe_2$ moiety assumes a position to serve as the recipient of methyl-bridging by one CH_3 group of the endocyclic $AlMe_2$ group: $d(Al_{endo}–CH_3)$ = 2.091 Å, $d(Al_{exo}–CH_3)$ = 2.223 Å. Interesting is the fact that there

exists a second cyclic minimum **5c** that is essentially isoenergetic with **5b**. Structure **5c** is C_s-symmetric, it contains *two* bridging methyl groups, the methyl bridges are asymmetric in the opposite direction compared to **5b**, that is, $d(Al_{endo}–CH_3) = 2.256$ Å > $d(Al_{exo}–CH_3) = 2.089$ Å.

The stationary structures of **5a**, **5b**, and **5c** are showed in the Figure 1, together with the transition state structure TSRF(**5a**,**5b**) for ring formation **5a** ⇄ **5b**, TSMT(**5b**,**5c**) for isomerization **5b** ⇄ **5c**, and ATS(**5c**) for automerization of **5c**. All the isomerization processes are facile even at low temperature. Hence, we conclude that cyclic **5b** is thermodynamically competitive and kinetically accessible.

Structures **5b** and **5c** can be viewed as the adducts of **7** and TMA. We previously discussed the formation of **7** via dimerization of **3** and the difficulty of generating **3** [32]. In this context, the formation of cyclic structures of **5** can be viewed as an "Umleitung" (German, detour) to a TMA adduct of **7** without going through **7**.

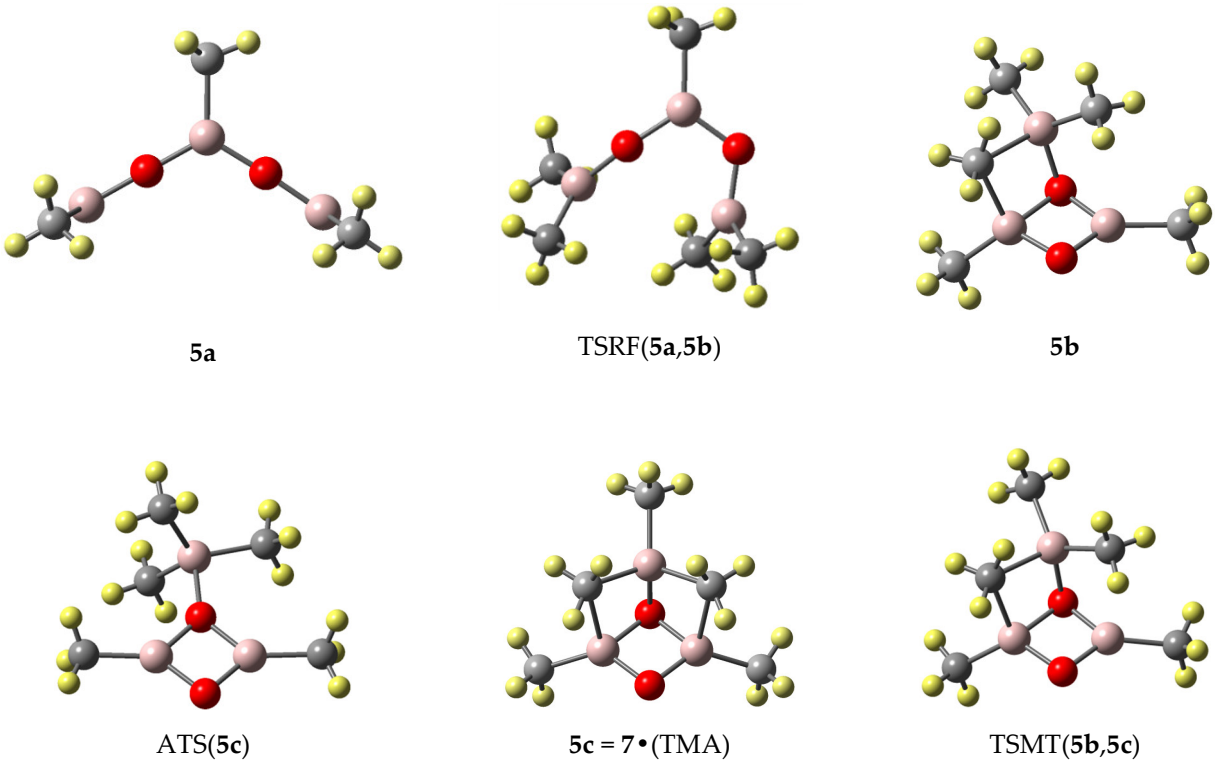

Figure 1. MP2/6-31G* optimized structures of permethyltrialuminoxane **5**: Acyclic allene structure **5a**, cyclic, monobridged structure **5b**, and cyclic, dibridged structure **5c**. Also shown are the computed structures of the transition state structures TSRF(**5a**,**5b**) for ring formation, of the transition state structure TSMT(**5b**,**5c**) for methyl transfer between **5b** and **5c**, and of the transition state structure ATS(**5c**) for automerization **5c** ⇄ **5c**.

2.2. Iron-Complexes: Dichlorides and Monochlorides

Here we report on the complexation of iron(II) complexes derived from complexes of the type $L(R_2)FeCl_2$ (Figure 2). The ligand $L(R)_2$ signifies a tridentate organic ligand and pyridine-2,6-diyldimethanimine (R = H) was considered as the parent organic tridentate ligand. Many of the organic ligands employed in Fe(II)/MAO catalyzed olefin polymerizations are *N*-aryl imines, and we studied the *N*,*N*-diphenyl ligand $L(Ph)_2$ and the *N*,*N*-dimethyl ligand $L(Me)_2$.

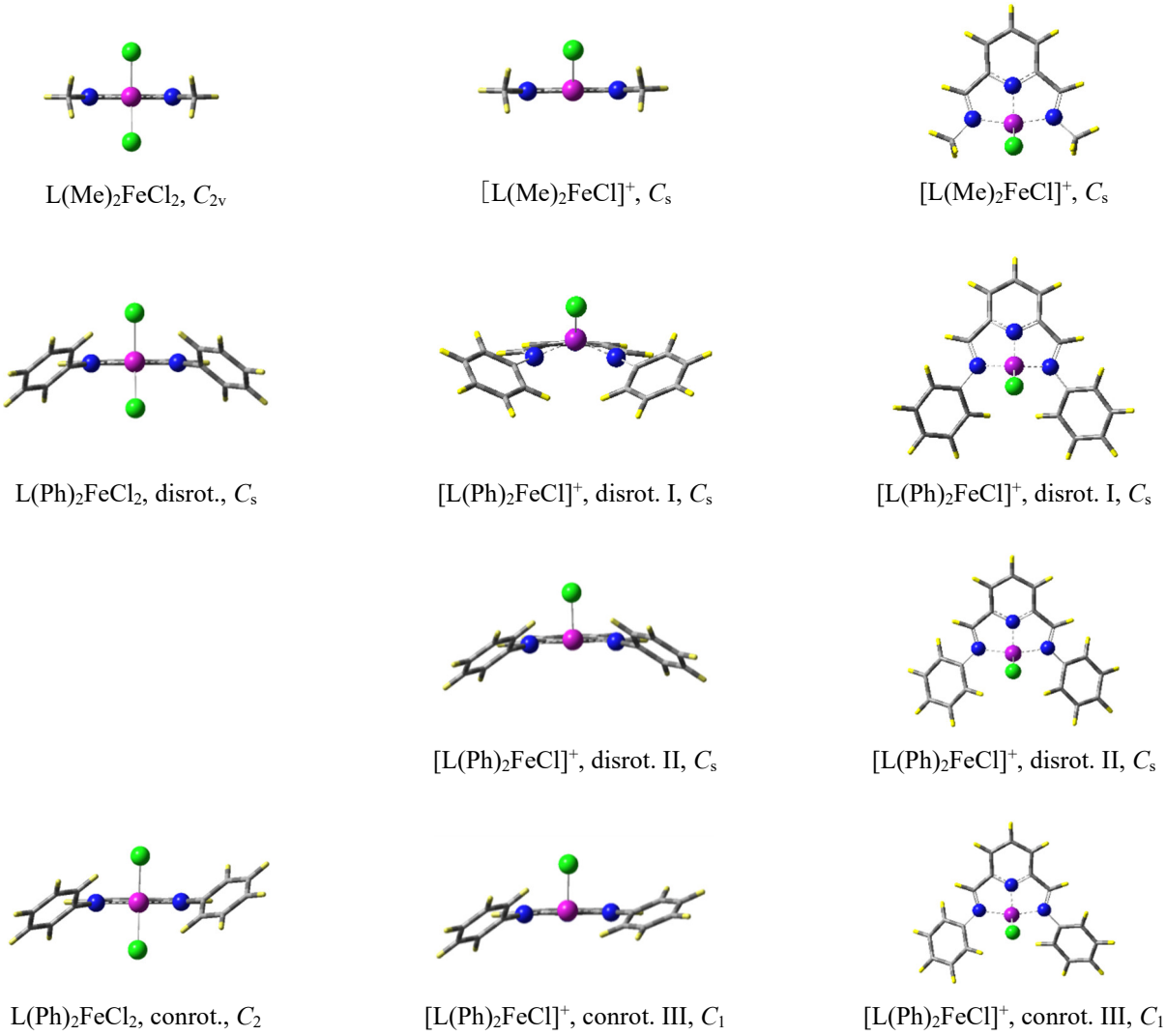

Figure 2. Iron dichloride pre-catalysts $L(R)_2FeCl_2$ are shown in the column on the left and two perspectives of the iron monochloride pre-catalysts $[L(R)_2FeCl]^+$ are shown in the other two columns.

The structures of dichloride complexes are shown in the first column of Figure 2. For $L(Me_2)FeCl_2$ there is one C_{2v} symmetric minimum. Two minima exist for complex $L(Ph_2)FeCl_2$ (Figure 2) depending as to whether the phenyl twists occur in the same (conrot., C_2) or in opposite (disrot., C_s) directions, and these complexes are essentially isoenergetic (Table 2).

It is thought that the dichloride complex is a pre-catalyst and that the dissociation of one chloride generates the cationic complex $[L(R_2)FeCl]^+$. The cationic complexes $[L(R_2)FeCl]^+$ (Figure 2) essentially retain the coordination geometry between iron and the organic ligand $L(R_2)$ as in the structure of the neutral dichloride complexes. There is one C_s-structure $[L(Me_2)FeCl]^+$ and two perspectives are shown in columns two and three of Figure 2. Isomers are possible for $[L(Ph_2)FeCl]^+$ depending on the conformation of the N–Ph bonds. In the monochloride, there are now *two* ways to obtain the minima with disrotatory N–Ph twists, I and II, in addition to the structure III resulting from conrotatory N–Ph twists. Structure I is slightly preferred over II and III (Table 2, top).

All structures of $[L(R)_2FeCl]^+$ feature chloride in pseudo-axial position and there are no minima in which chlorine would be placed in the best plane of the organic ligand. We found this observation significant and wanted to explore the possible origin. In Figure 3 are displayed the electrostatic potential maps of $[L(Me)_2FeCl]^+$ and the red and blue regions coincide with the location of the chlorine and iron, respectively. The iron center is the most

electrophilic site by far (dark blue region in Figure 3) and the perfect attractor for olefin monomers. The placement of the chloride ligand in the pseudo-axial position concentrates the iron electrophilicity with the additional advantage of minimizing steric interaction with the incoming olefin.

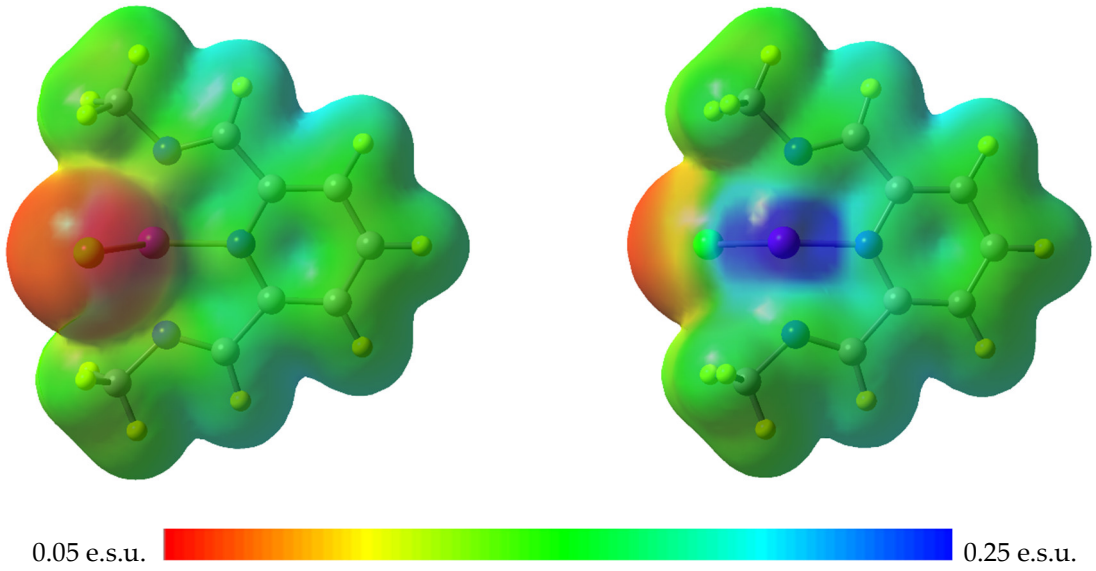

Figure 3. Electrostatic potential mapped on the electron density isosurface at ρ = 0.004 e/a.u.^{3} for the *N*,*N*-dimethyl system $[L(Me)_2FeCl]^+$. The surface map on the left shows the ligand face from the side of the axial chloride.

2.3. Iron-Complexation by Sinn Monomer **4**, *Cyclic Aluminoxane* **7**, *and Sinn Dimer* **5**

The iron dichloride complexes contain both chlorides in pseudo-axial positions, that is, the Fe–Cl directions are almost perpendicular to the LFe plane. Dissociation of one chloride leaves the other one in its pseudo-axial position in the $[L(R)_2FeCl]^+$ complexes (Figure 2). One might expect that the entry of a MAO ligand would occupy the pseudo-axial vacancy left by the removed chloride. Yet, as will be shown by the optimized structures below, this is not the case in any of $[L(R)_2FeCl(MAO)]^+$ complexes. Instead, the MAO species will occupy a pseudo-*equatorial* position so that it may act as a bidentate ligand engaging in O → Fe bonding and also in Cl → Al bonding. This mode of bidentate MAO coordination is illustrated in Scheme 4.

It is a significant advantage of this MAO coordination mode that the second pseudo-axial position remains vacant and ready for the coordination of an alkene. For the olefin polymerization to proceed by the mechanism outlined in the bottom row of Scheme 2, it is essential that the MAO species is placed next to the olefin, and this requires complexes of the type shown in Scheme 4 with an axial chlorine and an equatorial MAO species.

The desirable $[L(R)_2FeCl_{ax}(MAO)_{eq}]^+$ complexes compete with the isomeric $[L(R)_2FeCl_{eq}(MAO)_{ax}]^+$ complexes. These isomeric complexes also contain one O → Fe and one Cl → Al contact and one vacancy. However, the vacancy is next to the chloride rather than the MAO species.

We computed both the $[L(R)_2FeCl_{ax}(MAO)_{eq}]^+$ and $[L(R)_2FeCl_{eq}(MAO)_{ax}]^+$ complexes for the three MAO species **4**, **7** and **5b** for both the organic ligands $L(Ph)_2$ and $L(Me)_2$. Molecular models of optimized structures of these twelve complexes are shown in Figures 4–6 for **4**, **7** and **5b**, respectively. In each figure, the complexes with the $L(Ph)_2$ ligand are shown in the top row and the complexes in the left column contain equatorial chloride. The energies of the $[L(R)_2FeCl_{eq}(MAO)_{ax}]^+$ complex relative to the $[L(R)_2FeCl_{ax}(MAO)_{eq}]^+$ complex are included in Table 2, and the energetically preferred isomers are shown with green frames in the figures.

The MAO species **4** and **7** are symmetric and there is only one way for them to enter the coordination sphere of the $[L(R)_2FeCl_{ax}]^+$ complex. On the other hand, the ligand **5** is distinctly asymmetric. The structure of free **5** suggested that **5b** and **5c** as the best structural isomers with one or two methyl groups in a bridging position (Figure 1). However, in the complexes, the ligand has the topology of **5e** (Scheme 1), that is, the exocyclic $AlMe_2$ moiety is almost in the Al_2O_2 plane with the possibility of O → $AlMe_2$ dative bonding. This topology occurs in all four complexes with **5** (Figure 6). One of the in-ring Al atoms has only one methyl attached and coordinates to chloride (Al_a), while the other in-ring Al atom is bonded to two methyl groups (Al_b). For complex $L(Ph)_2FeCl_{ax}$(**5**)$_{eq}$, the distances involving Al_a are $d(Al_a–C)$ = 1.95 Å and $d(Al_a–Cl)$ = 2.34 Å, and the $d(Al_b–C)$ distances involving Al_b are 1.97 Å and 1.98 Å. The regiochemistry of the entry of **5** into the pre-catalyst $[L(R)_2FeCl_{ax}]^+$ is predetermined because chloride binds the Al_aMe moiety of the Al_2O_2 ring. Hence, the Al_bMe_2 moiety of the Al_2O_2 ring must be placed in the proximity of the vacancy, which is trans-apical with respect to chloride.

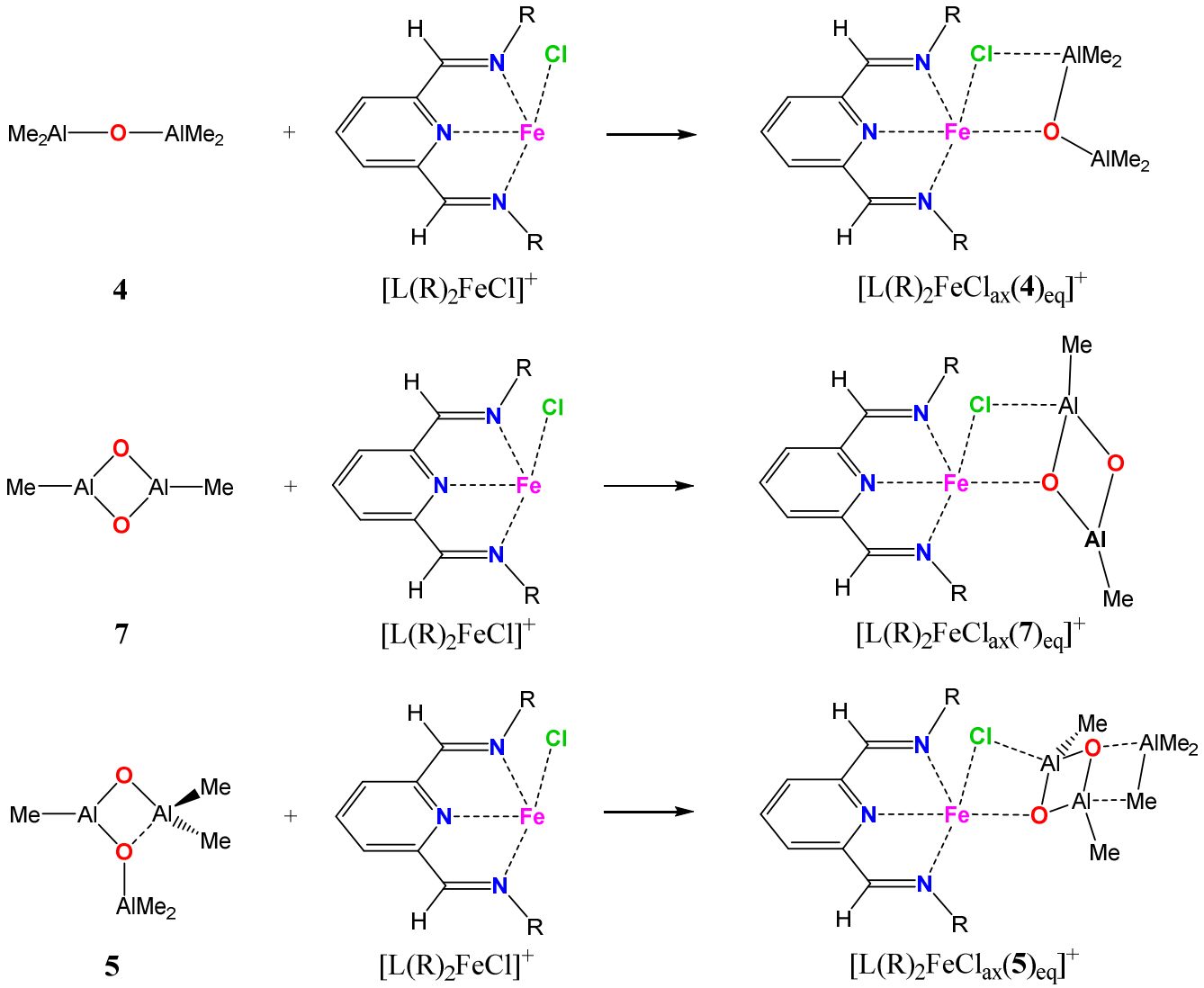

Scheme 4. The MAO Species Engages the Fe–Cl Bond as a Bidentate Donor-Acceptor Ligand.

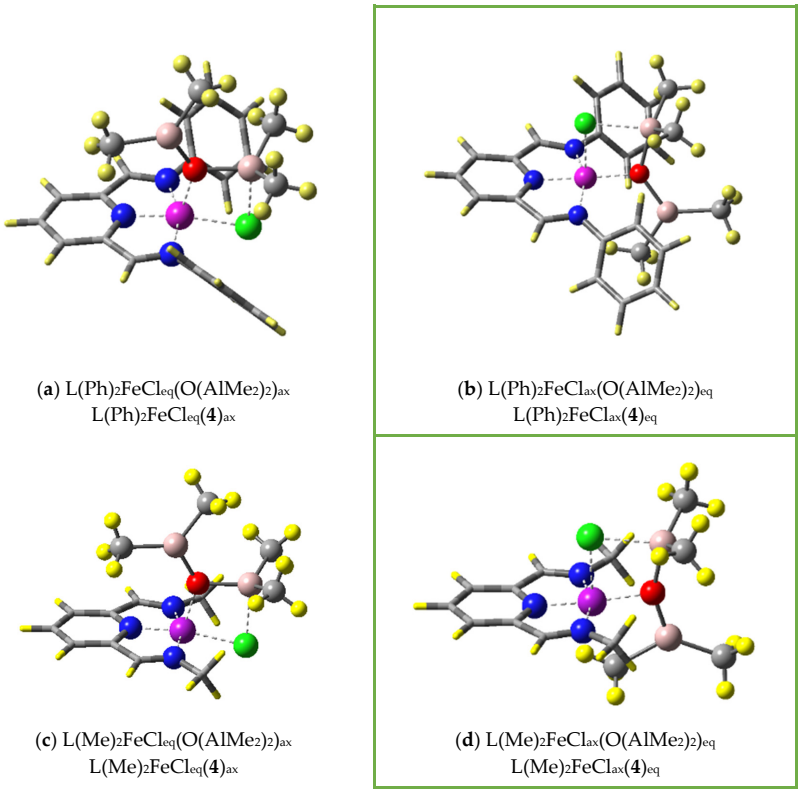

(**a**) $L(Ph)_2FeCl_{eq}(O(AlMe_2)_2)_{ax}$
$L(Ph)_2FeCl_{eq}(\mathbf{4})_{ax}$

(**b**) $L(Ph)_2FeCl_{ax}(O(AlMe_2)_2)_{eq}$
$L(Ph)_2FeCl_{ax}(\mathbf{4})_{eq}$

(**c**) $L(Me)_2FeCl_{eq}(O(AlMe_2)_2)_{ax}$
$L(Me)_2FeCl_{eq}(\mathbf{4})_{ax}$

(**d**) $L(Me)_2FeCl_{ax}(O(AlMe_2)_2)_{eq}$
$L(Me)_2FeCl_{ax}(\mathbf{4})_{eq}$

Figure 4. Computed structure of catalyst with the Sinn monomer **4**, $O(AlMe_2)_2$ a small acyclic aluminoxane. Top row: *N*,*N*-diphenyl ligand L; bottom row: *N*,*N*-dimethyl ligand L. Left column: equatorial chloride; right column: axial chloride.

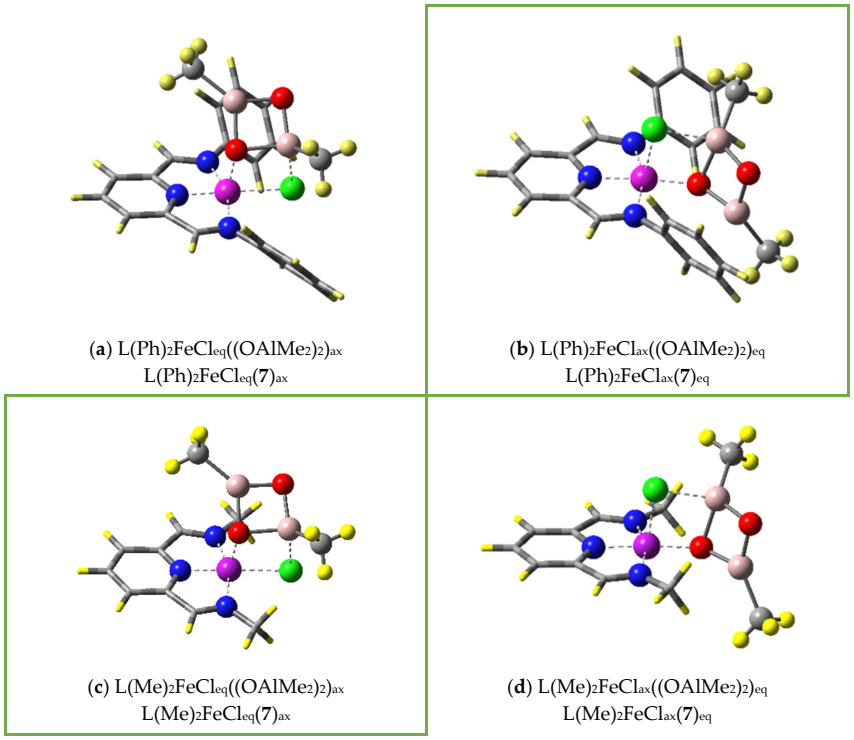

(**a**) $L(Ph)_2FeCl_{eq}((OAlMe_2)_2)_{ax}$
$L(Ph)_2FeCl_{eq}(\mathbf{7})_{ax}$

(**b**) $L(Ph)_2FeCl_{ax}((OAlMe_2)_2)_{eq}$
$L(Ph)_2FeCl_{ax}(\mathbf{7})_{eq}$

(**c**) $L(Me)_2FeCl_{eq}((OAlMe_2)_2)_{ax}$
$L(Me)_2FeCl_{eq}(\mathbf{7})_{ax}$

(**d**) $L(Me)_2FeCl_{ax}((OAlMe_2)_2)_{eq}$
$L(Me)_2FeCl_{ax}(\mathbf{7})_{eq}$

Figure 5. Computed structure of catalyst with **7**, $(OAlMe_2)_2$, a small cyclic aluminoxane. Top row: *N*,*N*-diphenyl ligand L; bottom row: *N*,*N*-dimethyl ligand L. Left column: equatorial chloride; right column: axial chloride.

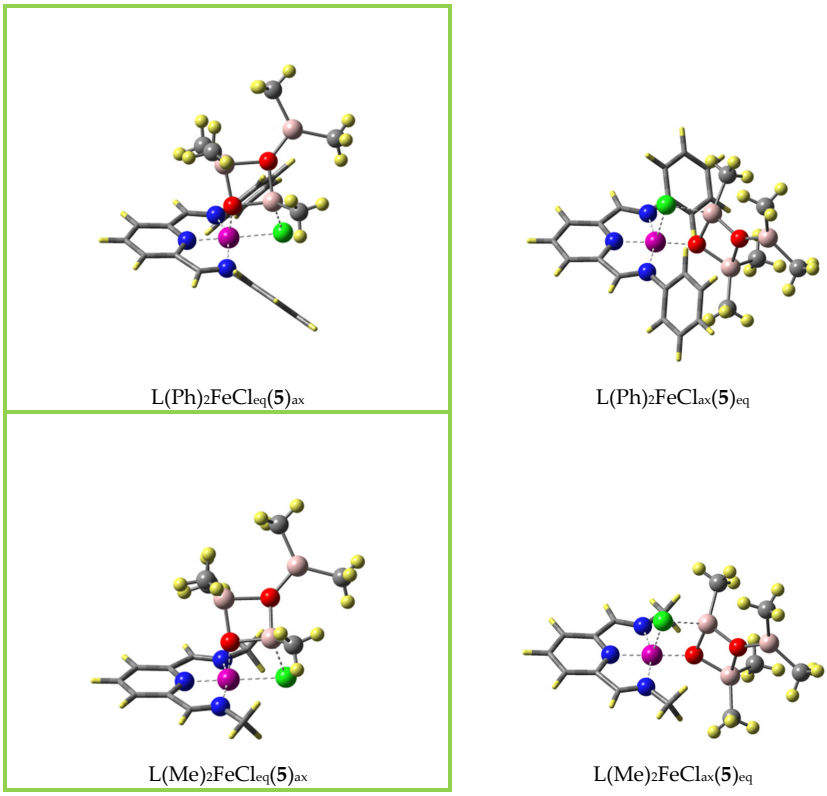

Figure 6. Computed structure of catalyst with **5**, the cyclic isomer of the Sinn trimer. Top row: *N*,*N*-diphenyl ligand L; bottom row: *N*,*N*-dimethyl ligand L. Left column: equatorial chloride; right column: axial chloride.

The structure of $L(Ph)_2FeCl_{ax}(\mathbf{5})_{eq}$ exemplifies perfectly the mechanism postulated in the bottom row of Scheme 2, that is, the idea that the MAO species *does not alkylate* the transition metal and instead *coordinates to* the transition metal. The regiochemistry of this coordination places the $AlMe_2$ moiety right next to the coordination site of an $H_2C{=}CH_2$ monomer and methyl transfer directly from the Al would result in the formation of an $Al(Me)(CH_2{-}CH_2{-}Me)$ moiety. The catalysis would continue to cycle, converting $Al(Me)([CH_2{-}CH_2]_n{-}Me)$ into $Al(Me)([CH_2{-}CH_2]_{n+1}{-}Me)$.

2.4. Kinetic vs. Thermodynamic Control of Complex Formation

We discussed the structure of the MAO complexed transition metal catalysts and our discussions emphasized the advantage of isomer $L(R)_2FeCl_{ax}(\mathbf{5})_{eq}$ for olefin polymerization. In Figures 3–5, the more stable isomers are highlighted by a green frame. As can be seen in Figure 4, there is a clear preference for the $L(R)_2FeCl_{ax}(\mathbf{4})_{eq}$ complexes with axial chloride irrespective of the nature of R. For the $L(R)_2FeCl(\mathbf{7})$ complexes in Figure 5, the complex with axial chloride is only preferred for the complex with the *N*,*N*-diphenyl ligand, $L(Ph)_2FeCl_{ax}(\mathbf{4})_{eq}$. This result provides guidance for the improvement of the organic ligand. The structure suggests that a cyclic Al_2O_2 system will tend to align with one *N*-arene group to benefit from parallel stacking. The interaction of the MAO species with the pre-catalyst will depend on the nature of the groups attached to the imine-*N*s and the core of the ligand, which determines the distance between the imines. Inspection of Figure 6 and the isomer stabilities in Table 2 show a preference for the $L(R)_2FeCl_{eq}(\mathbf{5})_{ax}$ complexes, even for the one with *N*-phenyl groups.

It is important to distinguish between thermodynamic and kinetic control of isomer formation. In Table 2, we do not only provide thermodynamic isomer stabilities (Reactions (4)–(6) and (13)–(15)), but we also provide the reaction energies for the addition of the MAO species **4**, **7**, and **5** to the pre-catalyst leading to the isomeric complexes

(Reactions (7)–(12) and (16)–(21)). The binding energies of the MAO species to iron are high and suggest irreversible MAO addition to the iron catalyst in fast reactions that will proceed without pronounced regioselectivity and not lead to thermodynamic equilibria. The positive consequence of this situation is that there will always be some active catalyst for the olefin polymerization. The art of catalyst design basically addresses the question as to how to provide a kinetic advantage for the formation of the desired $L(R)_2FeCl_{ax}(MAO)_{eq}$ isomer.

2.5. Absolute and Relative Oxophilicities and MAO Topology

The absolute oxophilicity Ω of the iron pre-catalyst $[L(R)_2FeCl]^+$ is defined as the negative of the binding energies of the MAO species which are given in Table 2, and we discuss the Δ*G* data. For example, the placement of **4**, **7**, and **5** in the equatorial position of $[L(Ph)_2FeCl]^+$ results in oxophilicities of 18.8 (R8), 35.4 (R10), and 35.0 (R12) kcal/mol, respectively. For the *N*-methyl species $[L(Me)_2FeCl]^+$, the respective numbers are 26.1 (R17), 36.5 (R19), and 41.3 (R21) kcal/mol respectively. These oxophilicities reflect the larger steric demand of the *N*-phenyl groups (decreasing Ω) and the opportunity for π stacking (increasing Ω).

We argued above that the oxygen in a cyclic aluminoxane would be a better donor in O → Fe dative bonding (Scheme 3). The results of the potential energy surface analysis allow to quantify this notion and we examined relative oxophilicities for MAO species in the equatorial position. The relative oxophilicity $\Omega_r(8,10)$ of the iron pre-catalyst $[L(Ph)_2FeCl]^+$ for cyclic **7** relative to acyclic **4** is given by the difference of the binding energies of reactions R8 and R10 in Table 2. In analogy, the relative oxophilicity $\Omega_r(8,12)$ specifies the preferences for cyclic **5** relative to acyclic **4** based on reactions R8 and R12. The values $\Omega_r(17,19)$ and $\Omega_r(17,21)$ are defined in the same way for the *N*-methyl ligand. The computed oxophilicities Ω_r are summarized in Table 3 and we discuss the Δ*G* values. The difference values $\Delta\Omega_r(10,12)$ and $\Delta\Omega_r(19,21)$ allow for a comparison of the two cyclic species **7** and **5**, and $\Delta\Omega_r < 0$ indicates that **5** is more strongly bonded ligand.

Table 3. Cyclic MAO are much Better Ligands Compared to Acyclic MAO Species (kcal/mol, B3LYP/6-31G*).

Oxophilicity Advantage	ΔE	ΔH_0	ΔH_{298}	ΔG_{298}
N-phenyl ligands $L(Ph)_2$				
Difference $\Omega_r(8,10)$	15.36	15.60	15.48	16.58
Difference $\Omega_r(8,12)$	10.81	11.62	10.72	16.17
Difference $\Delta\Omega_r(10,12)$	−4.55	−3.98	−4.76	−0.41
N-methyl ligands $L(Me)_2$				
Difference $\Omega_r(17,19)$	8.42	9.05	8.62	10.47
Difference $\Omega_r(17,21)$	9.98	10.96	9.94	15.22
Difference $\Delta\Omega_r(19,21)$	1.56	1.90	1.31	4.75

The Ω_r values all are greater than 10 kcal/mol, and in strong support of our hypothesis. Both **7** and **5** gave Ω_r values of $\Delta G \approx 16$ kcal/mol for the phenyl-substituted ligands with a small preference $\Delta\Omega_r(10,12)$. The respective Ω_r values for the methyl-substituted ligands are smaller and vary more; $\Delta G \approx 10$ kcal/mol for **7** and $\Delta G \approx 15$ kcal/mol for **5**, respectively.

2.6. Mechanistic Hypothesis and Suggested Experimental Approach

The traditional mechanism for MAO-assisted transition metal olefin polymerization considers the MAO species solely as to purveyor of methyl anion to generate an initial Fe–Me species and the turnover of the catalytical cycle keeps adding olefin to generate Fe–alkyl species as shown in Equation (1). We are proposing an alternative mechanism which can be summarized by Equation (2). It is the essential feature of this mechanism that the polymerization occurs at aluminum. The transition metal is directly bonded to aluminum

by way of an Fe–O–Al bridge and ensures that the iron-bonded olefin is positioned well for its aluminum-centered polymerization.

$$(H_2C{=}CH_2)LFe([CH_2\text{-}CH_2]_n\text{-}Me) \rightarrow LFe([CH_2\text{-}CH_2]_{n+1}\text{-}Me) \quad (1)$$

$$(H_2C{=}CH_2)LFe(Cl)\text{-}O\text{-}Al([CH_2\text{-}CH_2]_n\text{-}Me) \rightarrow LFe(Cl)\text{-}O\text{-}Al([CH_2\text{-}CH_2]_{n+1}\text{-}Me) \quad (2)$$

It is an essential feature of the proposed mechanism (Equation (2)) that the atoms of one Al–O bond of the MAO species coordinate both to the iron center and a remaining chloride ligand. This feature of the polymerization reaction described by Equation (2) is stressed in the bottom row of Scheme 2. The formation of O → Fe and Cl → Al dative bonds results in a four-membered ring, which should manifest itself in characteristic vibrational signatures. Therefore, we computed both the infrared and Raman intensities of the $L(R)_2FeCl_{ax}(X)_{eq}$ complexes with X = **4**, **5b**, and **7**. In Table S3 we compiled the vibrational modes composed of any combination of Fe–O, Fe–Cl, Al–O, and Al–Cl stretches. The visualization of molecular vibrations is not trivial, but depictions of atom displacement vectors associated with normal modes are beneficial. In Figure S4, we show atom displacement vectors of the three most characteristic vibrational modes of complex $L(R)_2FeCl_{ax}(\mathbf{5b})_{eq}$. We hope that these vibrational data encourage experimental studies.

3. Computational Methods

Computations were performed with *Gaussian09* [36] on the Lewis3 cluster [37] of the high-performance computing center at the University of Missouri. Potential energy surface (PES) analyses of the MAO species were performed with second-order Møller-Plesset perturbation theory (MP2) [38] with all electrons included in the active space and in conjunction with the 6-31G* basis set [39,40]. Vibrational analyses were carried out analytically for each stationary structure at the level of optimization to compute vibrational frequencies and molecular thermal energies, enthalpies, and entropies.

Considering the size of the complexes, the complexes were studied with density functional theory, the popular B3LYP hybrid functional [41], and with the 6-31G* basis set. The six *d*-electrons of Fe^{2+} are localized at the Fe center and their specific distribution has little effects on structures and complexation energies. We studied all systems as closed shell singlet using restricted Kohn-Sham orbitals.

4. Conclusions

We have presented the results of computational studies of the association of pre-catalysts $[L(Ph)_2FeCl]^+$ with three MAO species. We have shown that the oxygen in cyclic MAO species is a much better ligand in iron complexes compared to the oxygen in acyclic iron species. Importantly, the cyclic MAO species does not have to be a cycloaluminoxane such as $[(AlMe)O]_2$, **7** with all Al–O bonds being localized, but it can be an aluminoxane such as $(MeAl)[O(AlMe_2)]_2$, **5**, which adopts a cyclic structure because of intramolecular O → Al dative bonding.

It is thought that the pre-catalyst $L(R_2)FeCl_2$ goes through dissociation of one chloride and complexation of a MAO species to generate $[L(R)_2FeCl(MAO)]^+$ complexes with O → Fe and Cl → Al dative bonding. To enable olefin polymerization, the remaining chloride must be in the pseudo-axial position relative to the Fe-pyridine plane. According to our calculations, the $[L(R)_2FeCl_{ax}(MAO)_{eq}]^+$ complex formations are highly exothermic and exergonic (ΔG values of −19, −35, and −35 kcal/mol for MAO species **4**, **7**, and **5**, respectively), and the regiochemistry of their formation most likely is under kinetic control. Our study suggests that catalyst development should focus on the design of organic ligands (core and *N*-substituents) that will enhance the propensity for retaining one chloride in the axial position. Computed infrared and Raman spectra are reported and may guide experimental studies.

Supplementary Materials: The Supporting Information is available free of charge at https://www.mdpi.com/article/10.3390/catal12030312/s1, Tables S1 and S2 with the thermodynamic properties of MAO species and iron pre-catalysts, Table S3 with pertinent vibrational data, several figures related to the stationary structures of MAO species, illustrations of vibrational modes, and Cartesian coordinates of MAO species determined at the MP2(full)/6-31G* level and of all iron complexes determined at B3LYP/6-31G* level.

Author Contributions: Conceptualization, K.Y. and R.G.; Data curation, K.Y.; Funding acquisition, R.G.; Supervision, R.G.; Visualization, K.Y.; Writing—original draft, K.Y.; Writing—review & editing, R.G. All authors have read and agreed to the published version of the manuscript.

Funding: This research was funded by the petroleum Research Fund of the American Chemical Society grant number 53415-ND4, and, in part, by National Science Foundation grant number 1665487.

Data Availability Statement: Included in the Supplementary Materials.

Acknowledgments: This work was supported by the Missouri University of Science and Technology, by a grant from the Petroleum Research Fund of the American Chemical Society (#53415-ND4), and, in part, by a grant from the National Science Foundation #1665487.

Conflicts of Interest: The authors declare no competing financial interest.

References

1. Ziegler, K. Folgen und Werdegang einer Erfindung Nobel-Vortrag am 12. Dezember 1963. *Angew. Chem.* **1964**, *76*, 545–553. [CrossRef]
2. Natta, G. Von der Stereospezifischen Polymerisation zur Asymmetrischen Autokatalytischen Synthese von Makromolekülen Nobel-Vortrag am 12. Dezember 1963. *Angew. Chem.* **1964**, *76*, 553–566. [CrossRef]
3. Nowlin, T.E.; Mink, R.I.; Kissin, Y.V. Supported Magnesium/Titanium-Based Ziegler Catalysts for Production of Polyethylene. In *Handbook of Transition Metal Polymerization Catalysts*; John Wiley & Sons, Inc.: St. Hoboken, NJ, USA, 2010; pp. 131–155.
4. Severn, J.; Jones, R.L. Stereospecific α-Olefin Polymerization with Heterogeneous Catalysts. In *Handbook of Transition Metal Polymerization Catalysts*; John Wiley & Sons, Inc.: St. Hoboken, NJ, USA, 2010; pp. 157–230.
5. Sinn, H.; Kaminsky, W. Ziegler-Natta Catalysis. *Adv. Organomet. Chem.* **1980**, *18*, 99–149.
6. Andresen, A.; Cordes, H.G.; Herwig, J.; Kaminsky, W.; Merck, A.; Mottweiler, R.; Pein, J.; Sinn, H.; Vollmer, H.J. Halogen-Free Soluble Ziegler Catalysts for the Polymerization of Ethylene. Control of Molecular Weight by Choice of Temperature. *Angew. Chem.* **1976**, *88*, 689–690. [CrossRef]
7. Severn, J. Methylaluminoxane (MAO), Silica and a Complex: The "Holy Trinity" of Supported Single-Site Catalyst. In *Tailor-Made Polymers: Via Immobilization of Alpha-Olefin Polymerization Catalysts*; John Wiley & Sons, Inc.: St. Hoboken, NJ, USA, 2008; pp. 95–138.
8. Zaccaria, F.; Budzelaar, P.; Zuccaccia, C.; Cipullo, R.; Macchioni, A.; Busico, V.; Ehm, C. Chain Transfer to Solvent and Monomer in Early Transition Metal Catalyzed Olefin Polymerization: Mechanisms and Implications for Catalysis. *Catalysts* **2021**, *11*, 215. [CrossRef]
9. Kumar, S.; Dholakiya, B.; Jangir, R. Role of Organometallic Complexes in Olefin Polymerization: A Review Report. *J. Organomet. Chem.* **2021**, *953*, 122066. [CrossRef]
10. Köppl, A.; Alt, H.H.; Phillips, M.D. Partially Hydrolyzed Trimethylaluminum (PHT) as Heterogeneous Cocatalyst for the Polymerization of Olefins with Metallocene Complexes. *J. Appl. Polym. Sci.* **2001**, *80*, 454–466. [CrossRef]
11. Small, B.L.; Brookhart, M.; Bennett, A.M.A. Highly Active Iron and Cobalt Catalysts for the Polymerization of Ethylene. *J. Am. Chem. Soc.* **1998**, *120*, 4049–4050. [CrossRef]
12. Small, B.L.; Brookhart, M. Iron-Based Catalysts with Exceptionally High Activities and Selectivities for Oligomerization of Ethylene to Linear α-Olefins. *J. Am. Chem. Soc.* **1998**, *120*, 7143–7144. [CrossRef]
13. Ittel, S.D.; Johnson, L.K.; Brookhart, M. Late-Metal Catalysts for Ethylene Homo- and Copolymerization. *Chem. Rev.* **2000**, *100*, 1169–1203. [CrossRef]
14. Zhang, T.; Sun, W.H.; Li, T.; Yang, X. Influence of Electronic Effect on Catalytic Activity of Bis(imino)pyridyl Fe(II) and Bis(imino)pyrimidyl Fe(II) Complexes. *J. Mol. Catal. A* **2004**, *218*, 119–124. [CrossRef]
15. Zhang, S.; Sun, W.-H.; Xiao, T.; Hao, X. Ferrous and Cobaltous Chlorides Bearing 2,8-Bis(imino)quinolines: Highly Active Catalysts for Ethylene Polymerization at High Temperature. *Organometallics* **2010**, *29*, 1168–1173. [CrossRef]
16. Guo, D.; Han, L.; Zhang, T.; Sun, W.H.; Li, T.; Yang, X. Temperature Dependence of the Activity of a Late Transition Metal Catalyst by Molecular Modeling. *Macromol. Theory Simul.* **2002**, *11*, 1006–1012. [CrossRef]
17. Zhang, T.; Guo, D.; Jie, S.; Sun, W.H.; Li, T.; Yang, X. Influence of Electronic Effect on Catalytic Activity of Salicylaldiminato Nickel(II) Complexes. *J. Polym. Sci. Part A* **2004**, *42*, 4765–4774. [CrossRef]

18. Kong, S.; Guo, C.Y.; Yang, W.; Wang, L.; Sun, W.H.; Glaser, R. 2,6-Dibenzhydryl-N-(2-phenyliminoacenaphthylenylidene)-4-Chloroaniline nickel Dihalides: Synthesis, Characterization and Ethylene Polymerization for Polyethylenes with High Molecular Weights. *J. Organomet. Chem.* **2013**, *725*, 37–45. [CrossRef]
19. Lai, J.; Zhao, W.; Yang, W.; Redshaw, C.; Liang, T.; Liu, Y.; Sun, W.H. 2-[1-(2,4-Dibenzhydryl-6-methylphenylimino)ethyl]-6-[1-(arylimino)ethyl]pyridylcobalt(II) Dichlorides: Synthesis, Characterization and Ethylene Polymerization Behavior. *Polym. Chem.* **2012**, *3*, 787–793. [CrossRef]
20. Britovsek, G.J.P.; Bruce, M.; Gibson, V.C.; Kimberley, B.S.; Maddox, P.J.; Mastroianni, S.; McTavish, S.J.; Redshaw, C.; Solan, G.A.; Strömberg, S.; et al. Iron and Cobalt Ethylene Polymerization Catalysts Bearing 2,6-Bis(Imino)Pyridyl Ligands: Synthesis, Structures, and Polymerization Studies. *J. Am. Chem. Soc.* **1999**, *121*, 8728–8740. [CrossRef]
21. Zuo, W.; Sun, W.-H.; Zhang, S.; Hao, P.; Shiga, A. Highly Active Ethylene Polymerization and Copolymerization with Norbornene Using Bis(imino-indolide) Titanium Dichloride–MAO System. *J. Polym. Sci. Part A* **2007**, *45*, 3415–3430. [CrossRef]
22. Suzuki, Y.; Kinoshita, S.; Shibahara, A.; Ishii, S.; Kawamura, K.; Inoue, Y.; Fujita, T. Trimerization of Ethylene to 1-Hexene with Titanium Complexes Bearing Phenoxy−Imine Ligands with Pendant Donors Combined with MAO. *Organometallics* **2010**, *29*, 2394–2396. [CrossRef]
23. Velthoen, M.; Muñoz-Murillo, A.; Bouhmadi, A.; Cecius, M.; Diefenbach, S.; Weckhuysen, B. The Multifaceted Role of Methylaluminoxane in Metallocene-Based Olefin Polymerization Catalysis. *Macromolecules* **2018**, *51*, 343–355. [CrossRef]
24. Barron, A.R. A New Understanding of the Co-Catalytic Activity of Alumoxanes: The Opening of a Black Box! *Macromol. Symp.* **1995**, *97*, 15–25. [CrossRef]
25. Watanabi, M.; McMahon, C.N.; Harlan, C.J.; Barron, A.R. Reaction of Trimethylaluminum with $[(tBu)Al(\mu^3\text{-}O)]_6$: Hybrid *tert*-Butylmethylalumoxanes as Cocatalysts for Olefin Polymerization. *Organometallics* **2001**, *20*, 460–467. [CrossRef]
26. Pasynkiewicz, S. Alumoxanes: Synthesis, Structures, Complexes and Reactions. *Polyhedron* **1990**, *9*, 429–453. [CrossRef]
27. Sinn, H.J. Proposals for Structure and Effect of Methylalumoxane Based on Mass Balances and Phase Separation Experiments. *Macromol. Symp.* **1995**, *97*, 27–52. [CrossRef]
28. Zurek, E.; Woo, T.K.; Firman, T.K.; Ziegler, T. Modeling the Dynamic Equilibrium between Oligomers of $(AlOCH_3)n$ in Methylaluminoxane (MAO). A Theoretical Study Based on a Combined Quantum Mechanical and Statistical Mechanical Approach. *Inorg. Chem.* **2001**, *40*, 361–370. [CrossRef]
29. Negureanu, L.; Hall, R.W.; Butler, L.G.; Simeral, L.A. Methyaluminoxane (MAO) Polymerization Mechanism and Kinetic Model from Ab Initio Molecular Dynamics and Electronic Structure Calculations. *J. Am. Chem. Soc.* **2006**, *128*, 16816–16826. [CrossRef]
30. Linnolahti, M.; Severn, J.R.; Pakkanen, T.A. Formation of Nanotubular Methylaluminoxanes and the Nature of the Active Species in Single-Site α-Olefin Polymerization Catalysis. *Angew. Chem. Int. Ed.* **2008**, *47*, 9279–9283. [CrossRef]
31. Linnolahti, M.; Severn, J.R.; Pakkanen, T.A. Are Aluminoxanes Nanotubular? Structural Evidence from a Quantum Chemical Study. *Angew. Chem. Int. Ed.* **2006**, *45*, 3331–3334. [CrossRef]
32. Falls, Z.; Tyminska, N.; Zurek, E. The Dynamic Equilibrium Between $(AlOMe)_n$ Cages and $(AlOMe)_n{\cdot}(AlMe_3)_m$ Nanotubes in Methylaluminoxane (MAO): A First-Principles Investigation. *Macromolecules* **2014**, *47*, 8556–8569. [CrossRef]
33. Tyumkina, T.V.; Islamov, D.N.; Kovyazin, R.V.; Parfenovam, L.V. Chain and Cluster Models of Methylaluminoxane as Activators of Zirconocene Hydride, Alkyl, and Metallacyclopropane Intermediates in Alkene Transformation. *Mol. Catal.* **2021**, *512*, 111768. [CrossRef]
34. Glaser, R.; Sun, X. Thermochemistry of the Initial Steps of Methylaluminoxane Formation. Aluminoxanes and Cycloaluminoxanes by Methane Elimination from Dimethylaluminum Hydroxide and Its Dimeric Aggregates. *J. Am. Chem. Soc.* **2011**, *133*, 13323–13336. [CrossRef] [PubMed]
35. Zijlstra, H.S.; Harder, S. Methylalumoxane-History, Production, Properties, and Applications. *Eur. J. Inorg. Chem.* **2015**, 19–43. [CrossRef]
36. Frisch, M.J.; Trucks, G.W.; Schlegel, H.B.; Scuseria, G.E.; Robb, M.A.; Cheeseman, J.R.; Scalmani, G.; Barone, V.; Petersson, G.A.; Nakatsuji, H.; et al. Gaussian 09. 2016. Available online: https://gaussian.com/g09citation (accessed on 1 March 2022).
37. RCSS Documentation. Available online: http://docs.rnet.missouri.edu/lewis-and-clark-clusters (accessed on 1 March 2022).
38. Møller, C.; Plesset, M.S. Note on an Approximation Treatment for Many-Electron Systems. *Phys. Rev.* **1934**, *46*, 0618–0622. [CrossRef]
39. Petersson, G.A.; Bennett, A.; Tensfeldt, T.G.; Al-Laham, M.A.; Shirley, W.A.; Mantzaris, J. A Complete Basis Set Model Chemistry. I. The Total Energies of Closed-Shell Atoms and Hydrides of the First-Row Atoms. *J. Chem. Phys.* **1988**, *89*, 2193–2218. [CrossRef]
40. Petersson, G.A.; Al-Laham, M.A. A Complete Basis Set Model Chemistry. II. Open-shell Systems and the Total Energies of the First-Row Atoms. *J. Chem. Phys.* **1991**, *94*, 6081–6090. [CrossRef]
41. Lee, C.; Yang, W.; Parr, R.G. Development of the Colle-Salvetti Correlation-Energy Formula into a Functional of the Electron Density. *Phys. Rev. B* **1988**, *37*, 785–789. [CrossRef]